The Circulation of Metabolites in the Outer Retina

Daniel T. Hass[1], Elizabeth Giering[2], Celia M. Bisbach[3], Brian M. Robbings[1], Thomas O. Mundinger[2], and James B. Hurley[1,4]**

[1]Department of Biochemistry, 357350, University of Washington, Seattle, WA
[2]UW Diabetes Research Center, Seattle, WA
[3]Promega Corporation, Madison, WI
[4]Department of Ophthalmology, University of Washington, Seattle, WA

**Corresponding author: jbhhh@uw.edu

Keywords: Metabolism, infusion, isotopic, mass spectrometry, retina, RPE-choroid

Abstract

The posterior eye contains two metabolic microenvironments, each occupied by a distinct tissue type. Retinal pigment epithelium (RPE)-choroid tissue is connected to the circulatory system and receives plentiful O_2 and nutrients. Tight junctions formed by the RPE regulate the diffusion of nutrients to the neural retina. Retina tissue consequently exists in an environment with low O_2 levels and a lower variety of fuels that can support its metabolic needs. Retina explants release lactate and succinate, presumably as an adaptation to a low O_2 environment where they cannot be fully oxidized. The RPE-choroid is thought to aid retina metabolism by oxidizing these 'waste' products. We tested these ideas *in vivo* by infusing ^{13}C-labeled fuels through jugular vein catheters into circulation. By probing the patterns of ^{13}C labeling in glycolysis and the TCA cycle from different fuels and genetic models, we found that the retina and RPE do form a cooperative metabolic relationship, where the RPE-choroid oxidizes retina derived succinate but not lactate. Rather than consuming lactate, mouse RPE-choroid may act as a conduit for retina-derived lactate to re-enter circulation and feed more distant tissues.

Introduction

Not all cells in an organism are served directly by the circulatory system. In the posterior eye, the outer retina is an example. The source of metabolic support is circulation through a meshwork of fenestrated blood vessels, the choriocapillaris. Nutrients flow from these vessels through a collagenous layer (Bruch's membrane), then through a monolayer of cells, the retinal pigment epithelium (RPE), before reaching photoreceptors of the outer retina. Disorders that affect any step of this flow can deprive photoreceptors of fuel (1-4).

Despite their proximity to each other, photoreceptors and RPE cells occupy environments with very different access to O_2 (5, 6). O_2 levels are highest near RPE cells, which sit closest to the circulation, whereas O_2 levels are very low within the layer of photoreceptors. This reflects limited rate of O_2 diffusion through the tissue and the high level of O_2 consumption by both RPE cells and photoreceptor neurons.

Studies with isolated tissues have explored the idea that cells at different levels in this O_2 gradient use distinct metabolic strategies. Metabolic flux has been measured using isolated retina tissue and using a tissue preparation that comprises RPE and choroid. Those experiments indicate that energy metabolism in the retina and in the RPE-choroid are adapted to their native oxidative environments (7, 8). Photoreceptors can thrive in a limited O_2 supply by

consuming glucose rapidly and by releasing partially oxidized products, lactate and succinate, instead of fully oxidizing the carbons from glucose to CO_2. In contrast, isolated RPE-choroid tissue only sparingly uses glucose, but oxidizes lactate and succinate fully to CO_2.

So far, these ideas have only been tested by quantifying metabolic flux in isolated tissues. In this report we describe rigorous tests of the idea that these metabolic specializations and metabolite shuttling between tissues occurs *in vivo*. We followed flux of ^{13}C from labeled metabolites infused into the jugular veins of freely moving mice. We show that retina energy metabolism is fueled primarily by glucose and that it occurs chiefly in photoreceptors. Degeneration of photoreceptors greatly diminishes incorporation of ^{13}C from glucose into glycolytic and TCA cycle metabolites in the retina. The flow of ^{13}C-labelled lactate and succinate from the retina to the RPE-choroid is also diminished. Unexpectedly, we found that ^{13}C-lactate from the retina *in vivo* makes only a minor contribution to RPE-choroid TCA cycle metabolism, unlike in isolated RPE cells (8). These findings both confirm the presence of a synergistic metabolic relationship between the retina and RPE-choroid, but also amend our understanding of how these specialized tissues interact in a living organism.

Results and Discussion

A key feature of retina metabolism *ex vivo* is rapid consumption of glucose and production of lactate, even under aerobic conditions (8, 11-14). To determine whether this type of metabolism is also a feature of retinas *in vivo*, we infused mice with $^{13}C_6$-glucose and quantified the incorporation of ^{13}C into tissue metabolites. The metabolic path that $^{13}C_6$ (or m+6) -glucose takes and the labeling pattern it produces are indicated in **Fig. 1A**.

To probe metabolic relationships between retina and RPE-choroid *in vivo* we infuse ^{13}C-labeled fuels and quantify incorporation of ^{13}C into metabolic intermediates. We deliver the fuels by infusing them through jugular vein catheters into awake, freely moving mice. We sample plasma every 30 minutes through carotid artery catheters to determine when labeling in the plasma reaches steady-state. At steady-state we determine normalized labeling, the enrichment of a tissue metabolite relative to the enrichment of the circulating ^{13}C-labeled metabolite it is derived from (9, 10). “Normalized labeling” indicates the proportion of the metabolite in a tissue that is derived from the infused metabolite.

By 4 hours of infusion, m+6 glucose in plasma reaches steady-state (~20% of the glucose pool, **Fig.1B**). Notably, glucose is not the only circulating metabolite that is labeled. Unlabeled (m+0) fractions of plasma pyruvate, lactate, and other metabolites decay during the infusion period (**Fig S1A**). At 4 hours, the ~10% of lactate is m+3 labeled (produced by glycolysis of m+6 glucose) (**Fig. S1B**). At the same time, plasma citrate is composed of a mix of isotopologues derived from normal TCA cycle activity (m+2) and from pyruvate carboxylation (m+1, m+3) (**Fig. 1C**). Within tissues, labeling of lactate from infused glucose also approaches a steady-state (**Fig S1D**).

We compared the extent to which glucose from the plasma fuels production of downstream intermediates in the retina, cerebellum, RPE-choroid, liver, and plasma (**Fig.1C**). The normalized labeling of lactate quantifies the extent to which it is made by glycolysis directly from circulating glucose. A normalized labeling value of 1.0 means that 100% of lactate produced by the tissue is made by aerobic glycolysis of *glucose taken up directly from the blood*. Remarkably, the retina’s value for normalized lactate labeling is nearly 1.0 (0.975) (**Fig. 1C)**, higher than for any other tissue we evaluated. In all tissues other than retina, normalized

labeling of lactate is substantially less than 1 indicating that much of the lactate produced by those tissues is from other sources (gluconeogenesis or glycogen-derived glucose). We also measured normalized labeling of TCA cycle intermediates including citrate (**Fig. 1D**) and malate (**Fig. 1E**). Retina and cerebellum use blood glucose to make TCA cycle metabolites much more efficiently than liver and RPE-choroid (**Fig. 1D-E**).

Our *in vivo* analysis shows that circulating glucose is an excellent fuel for retinas but not for RPE-choroid (**Fig. 1**). RPE-choroid metabolism must instead rely on other fuels. The normal fuel preferences for this tissue are not known, but likely include lactate and succinate. Those metabolites are released by retina tissue explants and consumed by RPE-choroid explants (7, 8, 11, 13, 15, 16). As we had done with glucose, we determined the contribution of alternate fuels to tissue metabolism *in vivo*, using jugular vein infusions of $^{13}C_3$-lactate (**Fig. 2B**), $^{13}C_4$-succinate (**Fig. 2C**), $^{13}C_5$-glutamine (**Fig. 2D**), and $^{13}C_4$-malate (**Fig. 2E**). Each ^{13}C labeled fuel reached steady-state in plasma by 2 hours of infusion. For each infused fuel we measured labeling of 'nearby' metabolic intermediates (2-3 enzymatic steps away), to determine whether the infused fuel is integrated into downstream tissue metabolism (**Fig. 2. F-I**). Each fuel labeled downstream metabolic intermediates with a distinct tissue distribution.

We found that normalized labeling of m+2 citrate from infused m+3 lactate was more abundant in retina, cerebellum, and liver than in plasma (**Fig. 2F**). Based on that observation we think that some of the labeled TCA metabolites in tissues in ^{13}C glucose infusion experiments (**Fig. 1D,E**) are likely made from circulating m+3 lactate. Normalized labeling of $^{13}C_3$-lactate-derived m+2 citrate is similar in plasma and RPE-choroid (**Fig. 2F**). Based on that observation, it is possible that lactate is used directly in RPE-choroid to make m+2 citrate or that the labeled carbons of lactate are metabolized in other tissues, released into circulation as m+2 citrate and then imported into RPE-choroid.

Infused succinate, glutamine and malate do not contribute to metabolism as much as glucose or lactate. For example, circulating $^{13}C_4$-succinate and $^{13}C_4$-malate do not become TCA cycle intermediates in the retina, but do contribute to m+4 citrate pools in the RPE-choroid (**Fig. 2G, I**). A remarkable feature of the RPE-choroid is its capacity to import and oxidize all of the fuels we infused. Unlike the RPE-choroid, fuel use by the retina (and similarly the cerebellum) appeared more restricted.

While both glucose and other fuels are oxidized by retina explants (19-22), there has yet to be a direct comparison of how well the retina uses different fuels. We analyzed the ability of retinas to use these different fuels to label pyruvate, citrate, glutamate, and aspartate (**Fig. 2J-M**). Labeling of each metabolite in the retina was by far the highest when we infused $^{13}C_6$-glucose. Circulating $^{13}C_3$-lactate labels m+2 citrate in the retina about 2-fold more than in the RPE-choroid (**Fig. 2J-M**), but by comparing tissues labeled from $^{13}C_6$-glucose, we found that the preference for glucose as a fuel is even more pronounced in retinas compared to RPE-choroid (**Fig. 2J-M**). Infused glutamine, succinate or malate did not contribute substantially to retina mitochondrial metabolism.

The experiments in **Figures 1 and 2** do not directly label succinate, lactate, or other fuels from the retina but are used to different extents in each examined tissue. Expression of metabolite transporters on the retina-facing apical side may be different than on the plasma-facing basolateral side (17, 18). Therefore, we sought a different strategy to selectively label retina-derived metabolites and then determine their metabolic contribution to RPE-choroid metabolism.

To determine if products of glucose metabolism released from photoreceptors (succinate or lactate) can feed into metabolism in the RPE-choroid, we compared metabolism in the RPE-choroid of eyes in which the retina is normal to metabolism in the RPE-choroid of eyes in which photoreceptors have degenerated (**Fig. 3A**). The goal of making this comparison is to identify photoreceptor-derived metabolites that normally feed into the RPE-choroid but are missing when photoreceptors are not present.

Photoreceptors degenerate by one month of age in the eyes of mice with a deficiency of the chaperone protein, AIPL1 (23). Photoreceptors are metabolically active, so when they are absent, metabolic activity of the retina is diminished (24, 25). We hypothesized that loss of photoreceptors would cause a qualitative shift in the types of metabolic fuels used by the mutant retinas and in metabolites released from the retinas. To test this idea we catheterized AIPL1$^{-/-}$ mice (in a C57BL/6J background), infused them with $^{13}C_6$-glucose and then compared normalized metabolite labeling in the mutant retinas to age-matched C57BL/6J controls. We found that glucose still is the preferred metabolic substrate in AIPL1$^{-/-}$ retinas (**Fig. 3B**). Infusions performed over hours reflect the extent to which metabolism is fueled by a particular source. However, the absence of a change in substrate preference in the retina in long-term infusions experiments do not provide information about changes in the kinetics of fuel consumption and transfer of metabolites between tissues. To obtain this information we infused ^{13}C-glucose as a bolus (at 100 mg/kg) through jugular catheters, to identify differences rates of ^{13}C-glucose use *in vivo*.

In this type of infusion, fractional labeling of plasma m+6 glucose increases rapidly then decays as it is taken up by tissues (**Fig. S2A**). M+3 labeled lactate also instantly populates plasma and follows the opposite trend, rapidly appearing after the start of the infusion (**Fig. S2B**).

Incorporation of ^{13}C from glucose into tissue metabolites also increases and then decreases in response to the changes in supply of labeled fuel from the plasma. We collected retina and RPE-choroid tissue 1, 2, 3, and 5 minutes after the bolus infusion. “0 minute” samples are from unlabeled control mice. Following the $^{13}C_6$-glucose infusion, accumulation of ^{13}C is rapid. In the retinam pools of fully labeled (m+3) dihydroxyacetone phosphate (DHAP), 3-phosphoglycerate (3-PG), phosphoenolpyruvate (PEP), pyruvate, lactate, and citrate become saturated as soon as 1 minute following the bolus infusion (**Fig. S3A-E**). Unexpectedly, steady-state pools of all glycolytic intermediates in AIPL1$^{-/-}$ retinas are much larger than in C57BL/6J retinas. Because of this greater pool size, m+3 labeled DHAP, 3-PG, and PEP accumulate to much greater levels in AIPL1$^{-/-}$ retinas (**Fig. 3C-E**). Remarkably, the relative amounts of labeled metabolites inverted at the step in glycolysis where pyruvate kinase converts PEP into pyruvate. ^{13}C labeling of lactate and pyruvate made from glucose are much greater in C57BL/6J retinas (**Fig. 3F-G**). These findings show that without AIPL1, and therefore without photoreceptors, retinas do not complete glycolysis as quickly. This conclusion is supported by diminished labeling of TCA cycle and anapleurotic metabolites (**Fig. 3H-M**).

If metabolism in the retina feeds lactate and succinate to the RPE-choroid *in vivo*, then the diminished retinal metabolism in AIPL1$^{-/-}$ retinas should similarly diminish accumulation of ^{13}C-labeled intermediates in the RPE-choroid following a bolus infusion. We found that this does occur, but we also found that it is not the only change in RPE-choroid metabolism. Like in the retina, pools of glycolytic intermediates in the RPE-choroid are greater in size and also immediately saturate with ^{13}C following the bolus infusion (**Fig. S4A-E)**. This results in greater amounts of m+3 labeled DHAP, 3-PG, and PEP in the RPE-choroid of AIPL1$^{-/-}$ mice (**Fig. 4A-C**). Also like the retina, the accumulation of m+3 lactate and possibly m+3 pyruvate are slowed (**Fig. 4D-E**). However, whereas in the retina TCA cycle intermediates in AIPL1$^{-/-}$ are not

efficiently labeled, the early TCA intermediates do become labeled in RPE-choroid. Labeling of early TCA cycle intermediates is not affected by loss of m+3 lactate or increased m+3 glycolytic intermediates (**Fig. 4F-G**). However, labeled succinate and downstream malate and aspartate accumulate more slowly in the RPE-choroid when retina metabolism is impaired (**Fig. 4H-J**).

These differences in metabolism within the RPE-choroids of C57BL/6J and AIPL1$^{-/-}$ mice could result from intrinsic changes that occur in the RPE-choroid as a response to damage, such as an accumulation of immune cells or adaptation of RPE cells to the loss of photoreceptors. To address this possibility, we considered two possible explanations.

1. RPE-choroid metabolism in AIPL1$^{-/-}$ mice reflects changes intrinsic to that tissue, or
2. The intrinsic metabolic features of RPE-choroid are unchanged, but the changes in metabolism that we find *in vivo* are a consequence of being adjacent to a mutant retina that has altered metabolism.

If the metabolic changes we found reflect changes in glucose use intrinsic to the RPE-choroid, then an *ex vivo* incubation with $^{13}C_6$-glucose of RPE-choroid tissue freshly dissected from either C57BL/6J or AIPL1$^{-/-}$ eyes should replicate the differences we observed *in vivo*. Importantly, AIPL1 is not expressed in the RPE-choroid (26). We found (**Fig. 4K-T**) instead that intrinsic RPE-choroid metabolism is not affected by the loss of photoreceptors. Therefore, the most likely explanation for the findings is that shuttling of metabolites from the retina to the RPE-choroid is disrupted in AIPL1$^{-/-}$ eyes (**Fig. 4**).

Our findings indicate that succinate is both transported into the RPE-choroid from the circulation and also synthesized *de novo* by the retina and then transported to the RPE-choroid. In this *in vivo* analysis, we found evidence that succinate from the retina feeds the RPE-choroid. A decrease in retina-derived succinate in the RPE-choroid does impact downstream reactions and impedes the formation of malate. The magnitude of the decrease in succinate delivery to RPE-choroid due to the loss of photoreceptors was far lower than for lactate, suggesting that succinate is released from the retina but that not all succinate in the RPE originates from the retina. A portion of succinate comes from plasma, but our *ex vivo* experiments show that RPE-choroid tissue may also synthesize some of its own succinate.

Overall, our findings highlight and provide evidence for two important new concepts. The first is that of all the fuels that can feed energy to the retina, glucose and its products are by far the most prevalent. When $^{13}C_6$-glucose is supplied in circulation, 80% of citrate in the retina is m+2 labeled. Other TCA cycle intermediates are similarly labeled. Most of that labeling is from glycolysis in photoreceptors, but a minor fraction of it is from glucose-derived m+3 lactate or pyruvate in circulation. When the effects of lactate and pyruvate are subtracted, ~60.5% of retina metabolic flux (at the level of citrate) is derived directly from glucose. If the full contributions of glucose-derived lactate and pyruvate from plasma are included, we can account for 89.3% of retina metabolism. The remainder may be derived from non-esterified fatty acids such as palmitate, which are not only incorporated into photoreceptor outer segments (27), but which can, based on in *ex vivo* experiments, directly fuel retina energy metabolism *(19, 28)*.

The second highlight of this report relates to the metabolic interdependency of the retina and RPE-choroid. It already is clear that metabolism in the retina depends on metabolite transport through the retinal pigment epithelium (1, 3, 29), but our findings show that metabolism in the RPE-choroid also is affected by metabolism of the retina *in vivo*. Without photoreceptors, the RPE-choroid accumulates intermediates involved in glycolysis, but it is depleted of lactate and succinate. Unlike what would be predicted from our previous studies with cultured RPE cells

however, removing retina-derived ^{13}C-lactate from the RPE-choroid does not disrupt mitochondrial metabolism. Our findings suggest that while lactate from the retina is incorporated into RPE metabolism and can make amino acids such as alanine, it is not the most preferred energetic fuel for the RPE-choroid mitochondria, either when derived from circulation or from the retina. Instead, the high abundance of MCTs in the RPE may serve as a conduit for lactate to go out of the retina and into circulation. It is also possible that lactate could be used as a substrate for gluconeogenesis and possibly storage as glycogen.

Methods

Ethical approval

This study was carried out in accordance with the National Research Council's Guide for the Care and Use of Laboratory Animals (*8th ed*). All protocols were approved by the Institutional Animal Care and Use Committees at the University of Washington and the ACORP at the Veterans Affairs – Puget Sound Health Care System

Animals

All experiments used 2–5 month-old male and female wild-type C57BL/6J (RRID: IMSR_JAX:000664) mice, and Aipl1$^{-/-}$ mice bred to a C57BL/6J background over a series of at least six back-crosses. Mice were group housed at an ambient temperature of 25°C, with a 12-hour light cycle (6 am – 6 pm) and *ad libitum* access to water and normal rodent chow.

Surgery

The procedure for chronic jugular vein and carotid artery catheterization was performed as previously described (30) by the Metabolic and Cellular Phenotyping Core of the University of Washington's Diabetes Research Center. Briefly, following induction and maintenance under systemic inhaled anesthesia (isoflurane 1.5-2% in 1L/min), mice were administered with 4 mg/kg ketoprofen to reduce post-surgical swelling and provide analgesia. For intravenous infusions, jugular veins were isolated through a lateral incision to the trachea, and a silastic catheter was introduced into the vein, anchored to surrounding tissue, tunneled subcutaneously to the nape of the neck and connected to a vascular access port. A subset of mice received a contralateral carotid artery cannulation for blood sampling. The catheters were filled with heparinized saline, the skin incisions were sutured, and the mice recovered for 1 week before conscious infusion studies.

Infusions

We infused labeled fuels one of two ways. In the first way (**Fig. 1-2**) jugular catheters were infused gradually through syringes connected to syringe pumps. Metabolites were dissolved in sterile saline and infused at the concentrations and rates listed in table 1.

Table 1. Stock concentrations and infusion rates for 13C-labeled fuels.

Metabolite	Concentration (mM)	Infusion rate (µL/g/min)	Infusion period (min)	Supplier	Catalog #
$^{13}C_6$-glucose	200	0.1	240	Cambridge Isotope Laboratories	CLM-504
$^{13}C_3$-lactate	400	0.1	120		CLM-1579
$^{13}C_4$-succinate	10	0.05	120		CLM-1571
$^{13}C_5$-glutamine	100	0.1	120		CLM-1822-H
$^{13}C_4$-malate	10	0.05	120		CLM-8065-PK

Euthanasia and tissue dissection

Mice were all euthanized mice by awake cervical dislocation, followed by isolation of retina and RPE-choroid tissues. Mice were consistently euthanized 6-8 hours after light onset. To isolate the retina and RPE-choroid we enucleated the eye and trimmed away extraocular muscles. We removed the anterior segment of the eye by cutting at the ora serrata, then removed the lens. The remaining retina and RPE-choroid separate with minimal manipulation and were directly used in downstream experiments (*ex vivo* metabolic flux). Following infusion experiments, isolated tissue samples were flash frozen in liquid N_2.

Ex vivo metabolic flux
RPE-choroid tissue was incubated in Krebs-Ringer bicarbonate (KRB) buffer (98.5 mM NaCl, 4.9 mM KCl, 1.2 mM KH_2PO_4 1.2 mM $MgSO_4$-$7H_2O$, 20 mM HEPES, 2.6 mM $CaCl_2$-$2H_2O$, 25.9 mM $NaHCO_3$, pH 7.4) supplemented with 5 mM U-^{13}C-glucose. This buffer was equilibrated at 37°C, 21% O_2, and 5% CO_2 prior to incubations. We incubated freshly dissected RPE-choroid tissue in media at 37°C, 21% O_2, and 5% CO_2 for the indicated amounts of time. Following each incubation, tissue samples were flash frozen in liquid N_2.

Metabolite extraction
Metabolites were extracted in an extraction buffer consisting of 80% methanol, 20% H_2O, and 10 µM methylsuccinate (Sigma, M81209) as an internal standard. The extraction buffer was equilibrated on dry ice, and 150 µL was added to each sample. Tissues were then disrupted by sonication and incubated on dry ice for 45 minutes to precipitate protein. Proteins were pelleted at 17,000 × g for 30 minutes at 4°C. The supernatant containing metabolites was lyophilized at room temperature until dry and stored at −80°C until derivatization. The pellet containing protein was resuspended by sonication in RIPA buffer (150 mM NaCl, 1.0% Triton X-100, 0.5% sodium deoxycholate, 0.1% SDS, 50 mM Tris, pH 8.0) and protein was determined by a BCA assay (ThermoFisher, 23225).

Metabolite derivatization
Lyophilized samples were derivatized with 10 µL of 20 mg/mL methoxyamine HCl (Sigma, Cat#: 226904) dissolved in pyridine (Sigma, Cat#: 270970) and incubated at 37°C for 90 minutes. Samples were further derivatized with 10 µL tert-butyldimethylsilyl-N-methyltrifluoroacetamide (Sigma, 394882) and incubating at 70°C for 60 minutes.

Gas chromatography-mass spectrometry
Metabolites were analyzed on an Agilent 7890/5975C GC-MS using methods described extensively in previous work (8, 31). One microliter of derivatized sample is injected and delivered to an Agilent HP-5MS column by helium gas (flow rate: 1 mL/min). The column temperature starts at 100°C for 4 minutes then increases by 5°C/min to 300°C, where it is held for 5 min. We collect ion intensities after a 6.5-min solvent delay. Select ion monitoring (SIM) records only selected m/z in expected retention time windows. These masses range from m/z: ~50–600. Peaks were integrated in MSD ChemStation (Agilent), and correction for natural isotope abundance was performed using the software IsoCor (32, 33). Corrected metabolite signals were converted to molar amounts by comparing metabolite peak abundances in samples with those in a ‘standard mix’ containing known quantities of metabolites. Multiple concentrations of this mix were extracted, derivatized, and run alongside samples in each experiment.

Liquid chromatography-mass spectrometry
For liquid chromatography, samples were separated on an Acquity 2D UPLC equipped with an Acuity BEH Amide column (Waters, 2.1 × 50 mm, 1.7 µm). The mobile phases were (A) water with 10 mM ammonium acetate (pH 8.9) and (B) acetonitrile/water (95%/5%) with 10 mM ammonium acetate (pH 8.9). All solvents were LC–MS Optima grade (Fisher Scientific). The protocol was 0 min: [5% A, 95% B], 2 min [15% A, 85% B], 2.8 min: [40% A, 60% B], 3.2 min: [50% A, 50% B], 3.7 min: [15% A, 85% B], 4.4 min: [5% A, 95% B], at a flow rate of 0.4 mL/min**.** Chromatographically separated glucose was quantified on a Waters Xevo TQ mass spectrometer with electrospray ionization. Glucose ions were collected in negative mode with a cone = 18 V, collision energy = 8 V, parent ions of m/z = 179-185 and daughter ions of m/z=89-92. Dwell time for each ion was 0.08 s.

Statistical Analysis
We performed all statistical data analyses using Prism Version 9.5.1 (GraphPad Software). The significance threshold was set at 0.05. Data in all figures where individual points are not shown are displayed as mean ± SEM. Where individual data points are shown, bar graphs delineate mean ± SEM. “n” signifies sample size, which is indicated in figure legends for corresponding experiments.

Acknowledgements and Funding

J.B.H is supported by NEI RO1EY06641, RO1EY017863 and R21032597. DTH is supported by a Brightfocus Postdoctoral Fellowship (M2022003F). This work was supported in part by NIH NIDDK grant P30 DK017047 to the University of Washington Diabetes Research Center and used the Diabetes Research Center - Metabolic and Cellular Phenotyping Core.

Figure Legends

Figure 1. Glucose selectively fuels metabolism in the neural tissues. (A) A schematic representing the entry of $^{13}C_6$-glucose into tissue metabolism. ^{13}C (blue circles) occupies all of the carbons on glycolytic intermediates, and via acetyl-CoA labels two carbons on TCA cycle intermediates in the first round of the TCA cycle. **(B)** Isotopologues of glucose in plasma over the course of a 4 hour jugular vein infusion. M+6 and m+0 are the dominant glucose isotopologues, and during the infusion, m+0 glucose is gradually replaced by m+6 glucose. **(C)** Tissue m+3 lactate, **(D)** m+2 citrate, and **(E)** m+2 malate labeling relative to circulating m+6 glucose labeling. Labeling of retina and cerebellum are highest for all intermediates, demonstrating that most carbons on these intermediates primarily originate from glucose. Lactate is almost fully labeled from glucose in retina tissue, contrasting with other tissues that contain unlabeled lactate (n=4).

Figure 2. Glucose is utilized as a metabolic fuel more lactate, glutamine, succinate, or malate. (A) A schematic representing the entry of $^{13}C_6$-glucose, $^{13}C_3$-lactate, $^{13}C_5$-glutamine, $^{13}C_4$-succinate¸ and $^{13}C_4$-malate into tissue metabolism. In the TCA cycle, labeling patterns from glucose and lactate (blue) are identical, whereas ^{13}C labeling patterns of carbons from glutamine, succinate, and malate (pink) form a distinct labeling pattern. Plasma fractional labeling of **(B)** lactate (n=7), **(C)** succinate (n=4), **(D)** glutamine (n=4), and **(E)** malate (n=4) over the course of two-hour infusions demonstrates that plasma ^{13}C labeling is saturated at the final time point. The contribution of carbons from **(F)** lactate to citrate, **(G)** succinate to citrate, **(H)** glutamine to α-ketoglutarate, and (**I**) malate to citrate demonstrates that infused metabolites are integrated into tissue metabolism. Carbon atoms from circulating lactate and glutamine are integrated into downstream metabolites in a variety of tissues, whereas the integration of

succinate and malate into downstream metabolism was more restricted to the RPE-choroid. We quantified the ability of each infused fuel to label intermediates in the retina, including **(J)** pyruvate. **(K)** citrate, **(L)** glutamine, and **(M)** aspartate. Retina labeling from glucose was highest, followed by labeling from lactate. In contrast, carbon atoms from glutamine, succinate, and malate are poorly integrated into most intermediates in the retina.

Figure 3. Retina glucose flux but not glucose preference is impaired by degeneration. (A) A representation of the hypothesis motivating the experiments in Figures 3 and 4. Photoreceptors are sources of succinate and lactate. When photoreceptors degenerate the supply of succinate and lactate should be diminished. If retina-derived succinate and lactate fuel TCA cycle metabolism in the RPE-choroid, photoreceptor loss should deprive the RPE-choroid of fuel. **(B)** The hypothesis does not hold true if due to photoreceptor loss, retinas no longer use glucose. AIPL1$^{-/-}$ lose their photoreceptors by 1 month of age, and their preference for glucose as a metabolic fuel was determined using a four-hour infusion. Steady-state ^{13}C labeling after the infusion is comparable to C57BL/6J controls, suggesting that glucose is still the preferred fuel source in the remaining neural cells after photoreceptors have degenerated. To better determine whether the rate of retina metabolism was impaired by photoreceptor loss, we infused mice with a 10 mg/kg $^{13}C_6$-glucose bolus, through jugular catheters. We then followed integration of ^{13}C from glucose into downstream metabolites in retinas from C57BL/6J and AIPL1$^{-/-}$ mice. We determined labeling of intermediates from glycolysis, including **(C)** m+3 dihydroxyacetone-phosphate (DHAP), **(D)** m+3 3-phosphoglycerate (3-PG), **(E)** m+3 phosphoenolpyruvate (PEP), **(F)** m+3 pyruvate, and **(G)** m+3 lactate. Labeling of each intermediate is saturated, preventing a determination of ^{13}C accumulation rate. It is clear from this data that ^{13}C accumulates on before PEP and not downstream of PEP, suggesting a dysfunction in glycolysis when photoreceptors degenerate. This dysfunction appears to carry through to intermediates in the TCA cycle, as the rate of ^{13}C accumulation to form **(H)** m+2 citrate, **(I)** m+2 α-ketoglutarate, **(J)** m+2 glutamate, **(K)** m+2 succinate, **(L)** m+2 malate, and **(M)** m+2 aspartate is decreased over time (n=4-5 replicates/time point/genotype).

Figure 4. Impaired retina metabolic flux through the retina limits RPE-choroid metabolism. Impaired retina metabolism in AIPL1$^{-/-}$ mice alters the rate of ^{13}C accumulation on intermediates in the RPE-choroid from $^{13}C_6$-glucose. As in retinas, ^{13}C accumulates to a greater extent on (**A)** m+3 dihydroxyacetone-phosphate (DHAP), **(B)** m+3 3-phosphoglycerate (3-PG), and **(C)** m+3 phosphoenolpyruvate (PEP). Similarly, the % label on these intermediates is saturated (**Fig. S4**). (**D**) Whether the ability of 13C to form pyruvate is impaired is unclear, but **(E)** as in the retina there is far less m+3 lactate. Surprisingly, the decrease in labeled lactate does not correspond to a decrease in **(F)** m+2 citrate or **(G)** m+2 α-ketoglutarate. Unlike preceding metabolites, **(H)** m+2 succinate, **(I)** m+2 malate, and **(J)** m+2 aspartate are all decreased over time (n=4-5 replicates/time point/genotype). Differences in the mouse RPE-choroid due to AIPL1$^{-/-}$ could result from intrinsic changes in protein expression and not be mediated through the retina. To test this hypothesis, we also incubated RPE-choroid in 5 mM $^{13}C_6$-glucose *ex vivo* for 0, 1, 3, or 5 minutes (n=3-4 replicates/time point/genotype). Utilization of ^{13}C glucose *ex vivo* in glycolysis **(K-O)** or the TCA cycle **(P-T)** is unaffected by loss of AIPL1, suggesting that changes to RPE-choroid ^{13}C utilization in A-J are reactions to changes in retina metabolism.

References

1. Swarup A, Samuels IS, Bell BA, Han JYS, Du J, Massenzio E, et al. Modulating GLUT1 expression in retinal pigment epithelium decreases glucose levels in the retina: impact on photoreceptors and Müller glial cells. Am J Physiol Cell Physiol. 2019;316(1):C121-C33.
2. Curcio CA, Johnson M, Rudolf M, Huang JD. The oil spill in ageing Bruch membrane. Br J Ophthalmol. 2011;95(12):1638-45.
3. Wang W, Kini A, Wang Y, Liu T, Chen Y, Vukmanic E, et al. Metabolic Deregulation of the Blood-Outer Retinal Barrier in Retinitis Pigmentosa. Cell Rep. 2019;28(5):1323-34.e4.
4. Kurihara T, Westenskow PD, Gantner ML, Usui Y, Schultz A, Bravo S, et al. Hypoxia-induced metabolic stress in retinal pigment epithelial cells is sufficient to induce photoreceptor degeneration. Elife. 2016;5.
5. Yu DY, Cringle SJ. Oxygen distribution in the mouse retina. Invest Ophthalmol Vis Sci. 2006;47(3):1109-12.
6. Linsenmeier RA, Zhang HF. Retinal oxygen: from animals to humans. Prog Retin Eye Res. 2017;58:115-51.
7. Bisbach CM, Hass DT, Robbings BM, Rountree AM, Sadilek M, Sweet IR, et al. Succinate Can Shuttle Reducing Power from the Hypoxic Retina to the O2 Rich Pigment Epithelium. Cell Rep. 2020;31(5):107606.
8. Kanow MA, Giarmarco MM, Jankowski CS, Tsantilas K, Engel AL, Du J, et al. Biochemical adaptations of the retina and retinal pigment epithelium support a metabolic ecosystem in the vertebrate eye. Elife. 2017;6.
9. Hui S, Cowan AJ, Zeng X, Yang L, TeSlaa T, Li X, et al. Quantitative Fluxomics of Circulating Metabolites. Cell Metab. 2020;32(4):676-88.e4.
10. Hui S, Ghergurovich JM, Morscher RJ, Jang C, Teng X, Lu W, et al. Glucose feeds the TCA cycle via circulating lactate. Nature. 2017;551(7678):115-8.
11. Warburg O. The Metabolism of Carcinoma Cells. Cancer Research [Internet]. 1925 [cited 1; 9(1):[16 p.].
12. Ames A, Gurian BS. Effects of glucose and oxygen deprivation on function of isolated mammalian retina. J Neurophysiol. 1963;26:617-34.
13. Winkler BS. Glycolytic and oxidative metabolism in relation to retinal function. J Gen Physiol. 1981;77(6):667-92.
14. Wang L, Törnquist P, Bill A. Glucose metabolism in pig outer retina in light and darkness. Acta Physiol Scand. 1997;160(1):75-81.
15. Bisbach CM, Hass DT, Thomas ED, Cherry TJ, Hurley JB. Monocarboxylate Transporter 1 (MCT1) Mediates Succinate Export in the Retina. Invest Ophthalmol Vis Sci. 2022;63(4):1.
16. Hass DT, Bisbach CM, Robbings BM, Sadilek M, Sweet IR, Hurley JB. Succinate metabolism in the retinal pigment epithelium uncouples respiration from ATP synthesis. Cell Rep. 2022;39(10):110917.
17. Philp NJ, Wang D, Yoon H, Hjelmeland LM. Polarized expression of monocarboxylate transporters in human retinal pigment epithelium and ARPE-19 cells. Invest Ophthalmol Vis Sci. 2003;44(4):1716-21.
18. Chao JR, Knight K, Engel AL, Jankowski C, Wang Y, Manson MA, et al. Human retinal pigment epithelial cells prefer proline as a nutrient and transport metabolic intermediates to the retinal side. J Biol Chem. 2017;292(31):12895-905.
19. KEEN H, CHLOUVERAKIS C. METABOLISM OF ISOLATED RAT RETINA. THE ROLE OF NON-ESTERIFIED FATTY ACID. Biochem J. 1965;94(2):488-93.
20. Du J, Cleghorn WM, Contreras L, Lindsay K, Rountree AM, Chertov AO, et al. Inhibition of mitochondrial pyruvate transport by zaprinast causes massive accumulation of aspartate at the expense of glutamate in the retina. J Biol Chem. 2013;288(50):36129-40.

21. Chertov AO, Holzhausen L, Kuok IT, Couron D, Parker E, Linton JD, et al. Roles of glucose in photoreceptor survival. J Biol Chem. 2011;286(40):34700-11.
22. Li B, Zhang T, Liu W, Wang Y, Xu R, Zeng S, et al. Metabolic Features of Mouse and Human Retinas: Rods versus Cones, Macula versus Periphery, Retina versus RPE. iScience. 2020;23(11):101672.
23. Singh RK, Kolandaivelu S, Ramamurthy V. Early alteration of retinal neurons in Aipl1-/- animals. Invest Ophthalmol Vis Sci. 2014;55(5):3081-92.
24. Du J, Rountree A, Cleghorn WM, Contreras L, Lindsay KJ, Sadilek M, et al. Phototransduction Influences Metabolic Flux and Nucleotide Metabolism in Mouse Retina. J Biol Chem. 2016;291(9):4698-710.
25. Hass DB, Celia Sadilek, Martin Sweet, Ian Hurley, James. Aerobic Glycolysis in Photoreceptors Supports Energy Demand in the Absence of Mitochondrial Coupling. 19 ed. Ash J, Pierce E, Anderson R, Bowes Rickman Ca, Hollyfield Jo, Grimm C, editors: Springer Nature; 2023.
26. van der Spuy J, Chapple JP, Clark BJ, Luthert PJ, Sethi CS, Cheetham ME. The Leber congenital amaurosis gene product AIPL1 is localized exclusively in rod photoreceptors of the adult human retina. Hum Mol Genet. 2002;11(7):823-31.
27. Wang N, Anderson RE. Synthesis of docosahexaenoic acid by retina and retinal pigment epithelium. Biochemistry. 1993;32(49):13703-9.
28. Joyal JS, Sun Y, Gantner ML, Shao Z, Evans LP, Saba N, et al. Retinal lipid and glucose metabolism dictates angiogenesis through the lipid sensor Ffar1. Nat Med. 2016;22(4):439-45.
29. Han JYS, Kinoshita J, Bisetto S, Bell BA, Nowak RA, Peachey NS, et al. Role of monocarboxylate transporters in regulating metabolic homeostasis in the outer retina: Insight gained from cell-specific Bsg deletion. FASEB J. 2020;34(4):5401-19.
30. Ayala JE, Bracy DP, Malabanan C, James FD, Ansari T, Fueger PT, et al. Hyperinsulinemic-euglycemic clamps in conscious, unrestrained mice. J Vis Exp. 2011(57).
31. Du J, Linton JD, Hurley JB. Probing Metabolism in the Intact Retina Using Stable Isotope Tracers. Methods Enzymol. 2015;561:149-70.
32. Millard P, Delépine B, Guionnet M, Heuillet M, Bellvert F, Létisse F. IsoCor: isotope correction for high-resolution MS labeling experiments. Bioinformatics. 2019;35(21):4484-7.
33. Millard P, Letisse F, Sokol S, Portais JC. IsoCor: correcting MS data in isotope labeling experiments. Bioinformatics. 2012;28(9):1294-6.

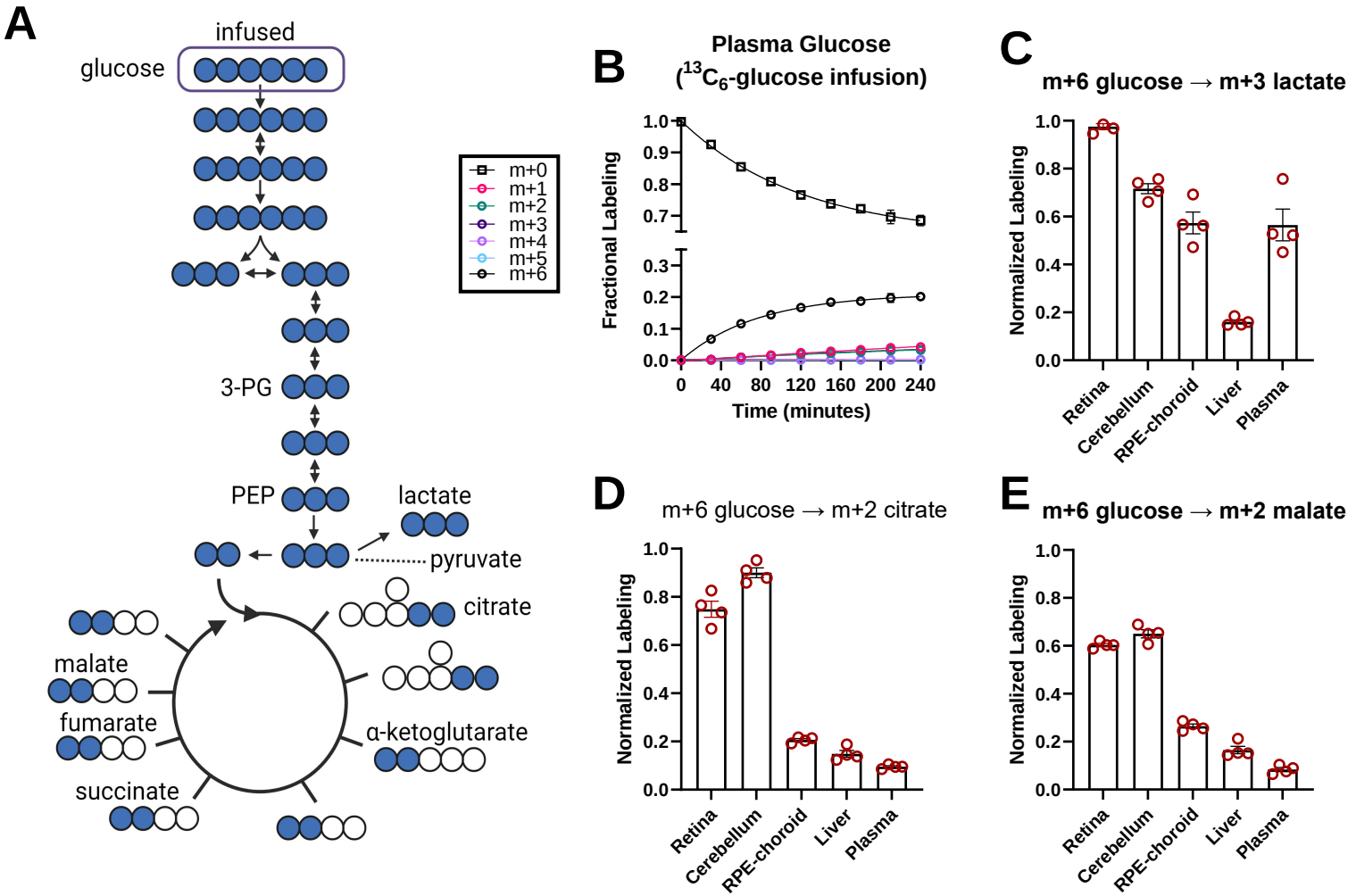
A
infused
glucose
3-PG
PEP
lactate
pyruvate
citrate
malate
fumarate
α-ketoglutarate
succinate
m+0
m+1
m+2
m+3
m+4
m+5
m+6
B
Plasma Glucose
($^{13}C_6$-glucose infusion)
Fractional Labeling
Time (minutes)
C
m+6 glucose → m+3 lactate
Normalized Labeling
Retina
Cerebellum
RPE-choroid
Liver
Plasma
D
m+6 glucose → m+2 citrate
Normalized Labeling
E
m+6 glucose → m+2 malate
Normalized Labeling

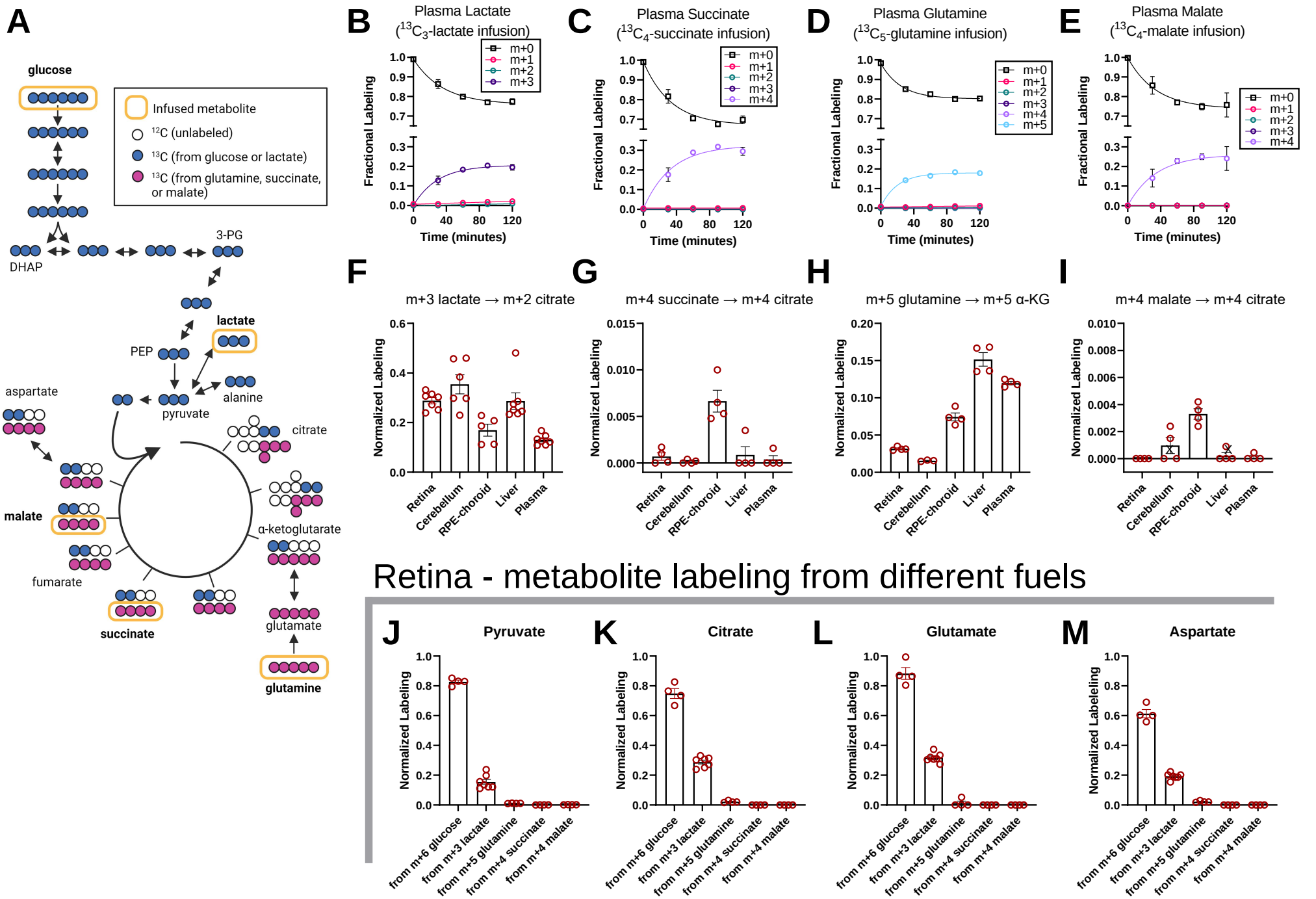
A
glucose
Infused metabolite
12C (unlabeled)
13C (from glucose or lactate)
13C (from glutamine, succinate, or malate)
DHAP
3-PG
lactate
PEP
alanine
pyruvate
aspartate
citrate
malate
α-ketoglutarate
fumarate
succinate
glutamate
glutamine
B
Plasma Lactate
(13C3-lactate infusion)
C
Plasma Succinate
(13C4-succinate infusion)
D
Plasma Glutamine
(13C5-glutamine infusion)
E
Plasma Malate
(13C4-malate infusion)
m+0
m+1
m+2
m+3
m+4
m+5
Fractional Labeling
Time (minutes)
F
m+3 lactate → m+2 citrate
G
m+4 succinate → m+4 citrate
H
m+5 glutamine → m+5 α-KG
I
m+4 malate → m+4 citrate
Normalized Labeling
Retina
Cerebellum
RPE-choroid
Liver
Plasma
Retina - metabolite labeling from different fuels
J
Pyruvate
K
Citrate
L
Glutamate
M
Aspartate
Normalized Labeling
from m+6 glucose
from m+3 lactate
from m+5 glutamine
from m+4 succinate
from m+4 malate

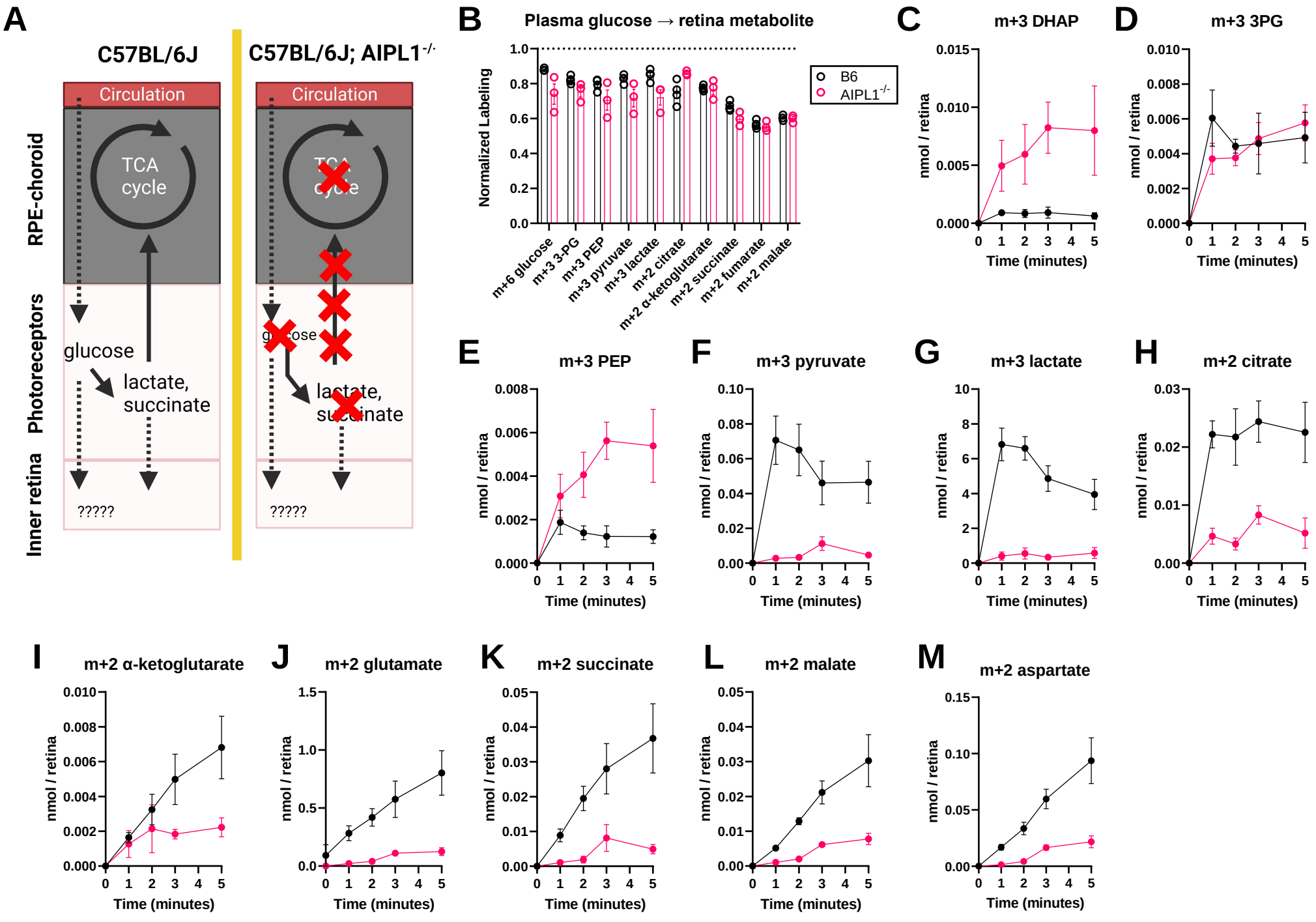
A
C57BL/6J
C57BL/6J; AIPL1-/-
Circulation
TCA cycle
RPE-choroid
Photoreceptors
Inner retina
glucose
lactate, succinate
?????
B
Plasma glucose → retina metabolite
Normalized Labeling
B6
AIPL1-/-
m+6 glucose
m+3 3-PG
m+3 PEP
m+3 pyruvate
m+3 lactate
m+2 citrate
m+2 α-ketoglutarate
m+2 succinate
m+2 fumarate
m+2 malate
C
m+3 DHAP
D
m+3 3PG
E
m+3 PEP
F
m+3 pyruvate
G
m+3 lactate
H
m+2 citrate
I
m+2 α-ketoglutarate
J
m+2 glutamate
K
m+2 succinate
L
m+2 malate
M
m+2 aspartate
nmol / retina
Time (minutes)

RPE-choroid: **C57BL/6J** vs. **AIPL1$^{-/-}$**

in vivo *- the retina can supply fuels*

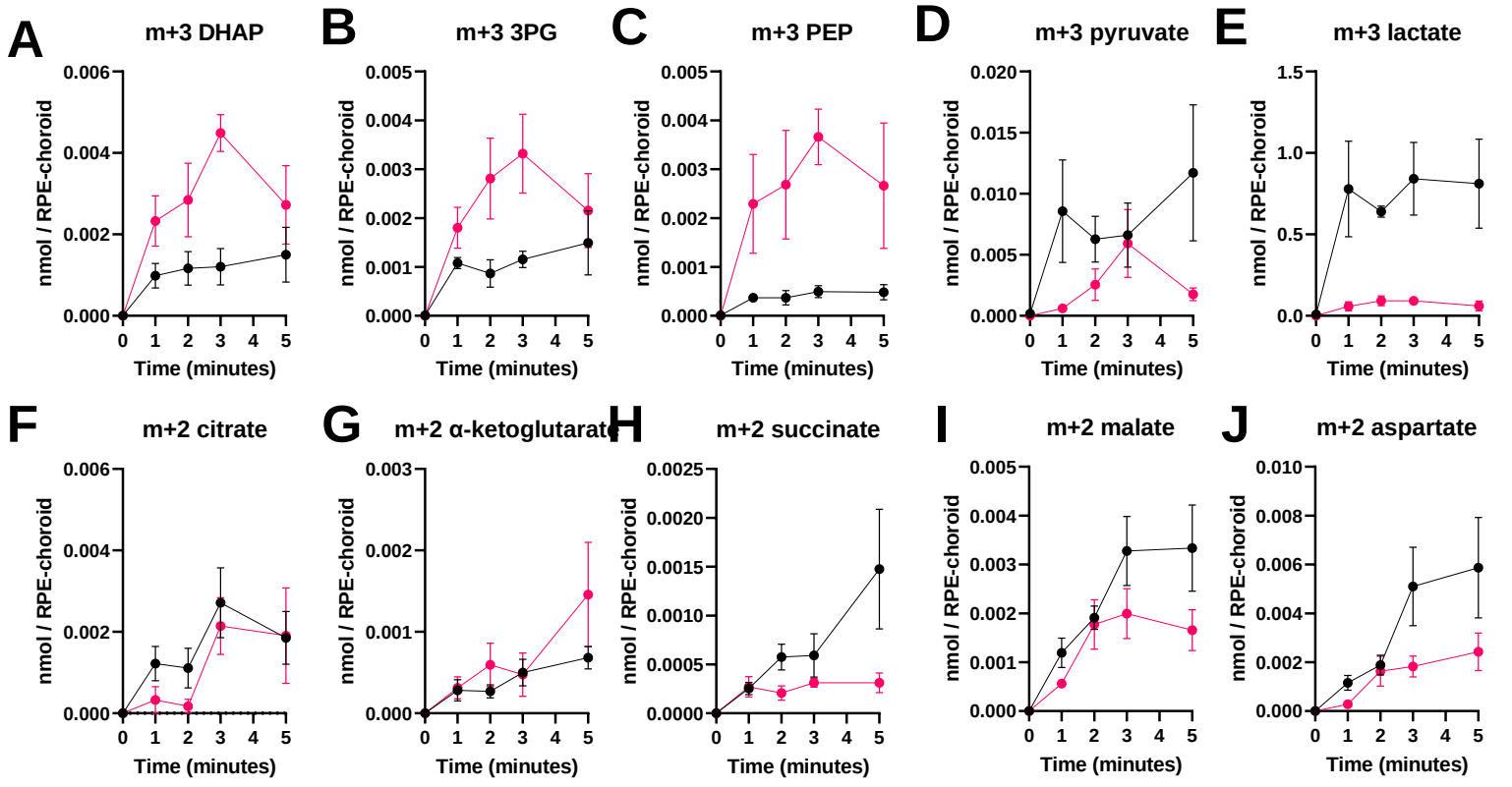
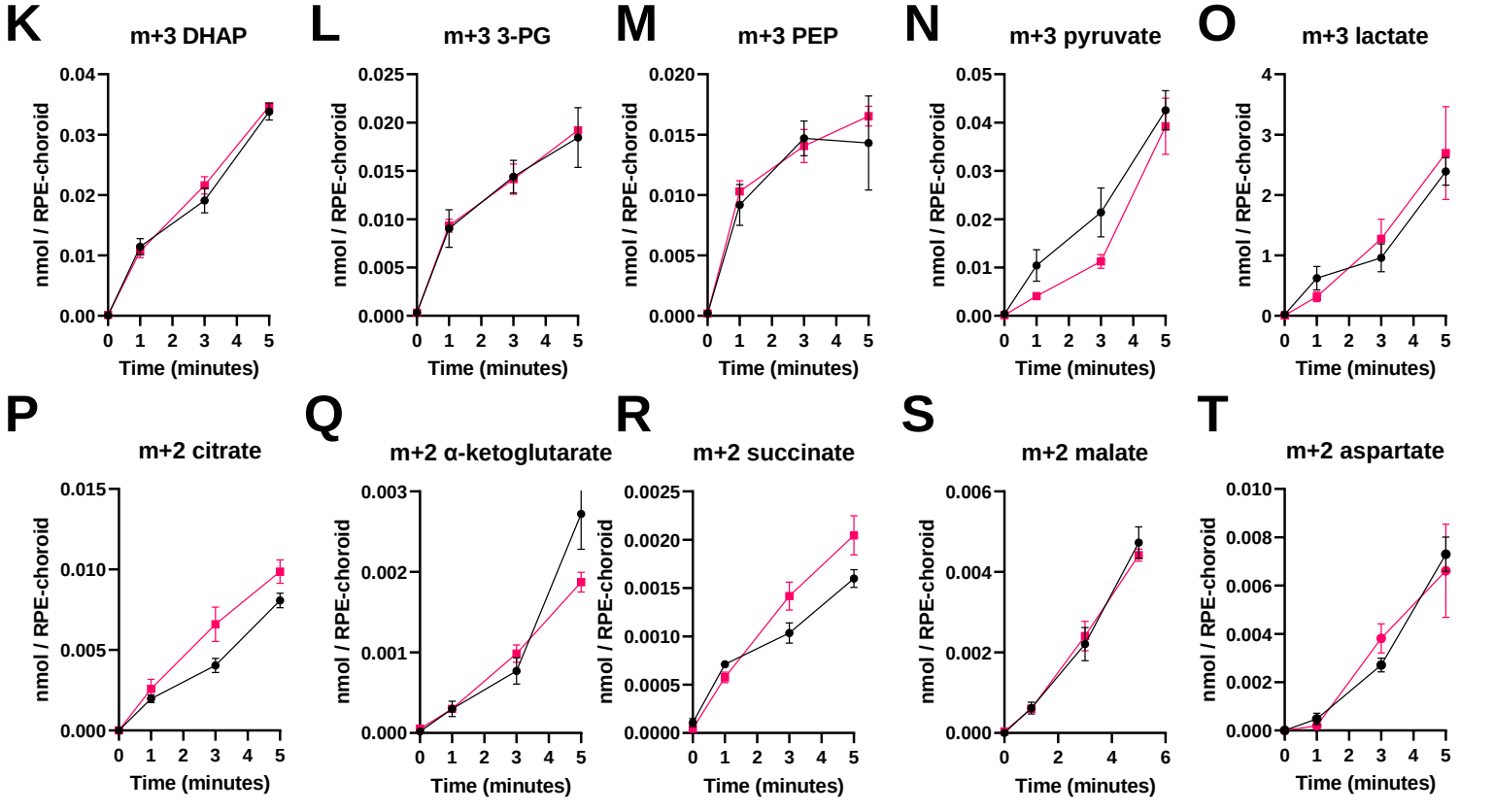
ex vivo *- the retina is not present*